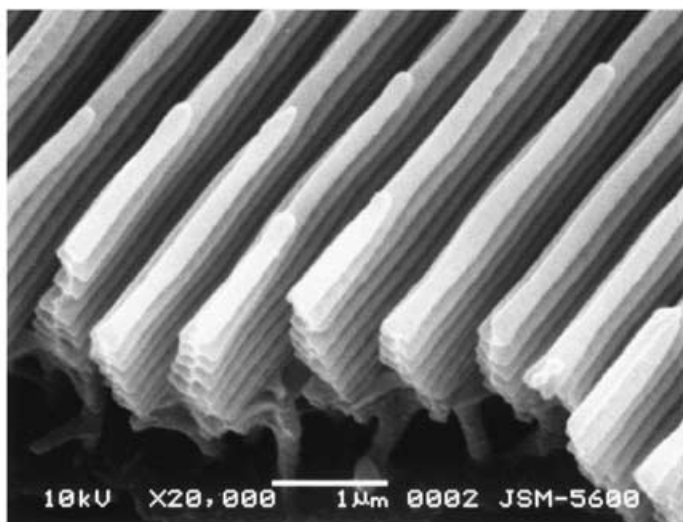
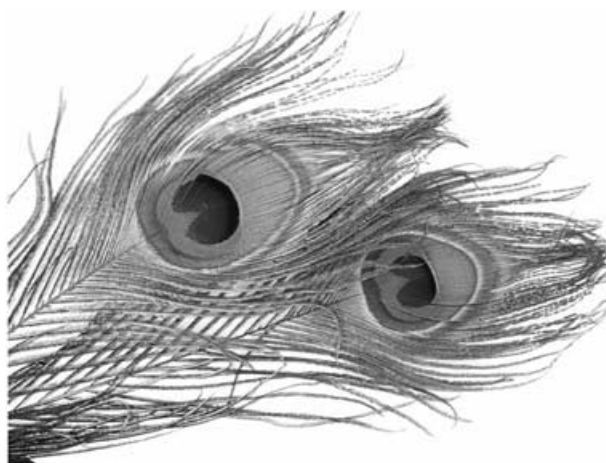


Structural Colors in Nature:  
The Role of Regularity and  
Irregularity in the Structure



# Structural Colors in Nature: The Role of Regularity and Irregularity in the Structure

Shuichi Kinoshita\* and Shinya Yoshioka<sup>[a]</sup>

*Coloring in nature mostly comes from the inherent colors of materials, but it sometimes has a purely physical origin, such as diffraction or interference of light. The latter, called structural color or iridescence, has long been a problem of scientific interest. Recently, structural colors have attracted great interest because their applications have been rapidly progressing in many fields related to vision, such as the paint, automobile, cosmetics, and textile industries. As the research progresses, however, it has become clear that these colors are due to the presence of surprisingly minute microstructures, which are hardly attainable even by ultramodern nanotechnology. Fundamentally, most of the structural colors originate from basic optical processes represented by thin-film interference, multilayer interference, a diffraction grating effect, photonic crystals, light scattering, and so on. How-*

*ever, to enhance the perception of the eyes, natural creatures have produced various designs, in the course of evolution, to fulfill simultaneously high reflectivity in a specific wavelength range and the generation of diffusive light in a wide angular range. At a glance, these two characteristics seem to contradict each other in the usual optical sense, but these seemingly conflicting requirements are realized by combining appropriate amounts of regularity and irregularity of the structure. In this Review, we first explain the fundamental optical properties underlying the structural colors, and then survey these mysteries of nature from the viewpoint of regularity and irregularity of the structure. Finally, we propose a general principle of structural colors based on structural hierarchy and show their up-to-date applications.*

## 1. Introduction

The study of structural colors has a long history. Probably the oldest scientific descriptions of structural colors were those in *Micrographia*,<sup>[1]</sup> written by Hooke in 1665. In this book, he investigated brilliant feathers of the peacock and duck using a microscope, and found that their colors were destroyed by a drop of water. He speculated that alternate layers of thin plates and air strongly reflected the light. Newton described in *Opticks* that the colors of the iridescent peacock arose from the thinness of the transparent part of the feathers.<sup>[2]</sup> However, the further scientific development of structural colors had to wait for the establishment of electromagnetic theory by Maxwell in 1873 and also for the experimental study of electromagnetic waves by Hertz in 1884. After this, the fundamental properties of light, such as reflection, refraction, and polarization characteristics, could be quantitatively treated, and the studies on structural colors proceeded rapidly but in an unexpected direction: a significant conflict arose between “surface colors” and “structural colors”, which divided the world of physics in two.

In the early 1900s, the general idea for structural colors was not that of optical interference, which Hooke and Newton had implied, but that proposed by Walter in 1895.<sup>[3]</sup> He insisted that metallic colors in nature were due to reflection from a surface involving pigments and called “surface colors”. He explained that the variation of colors with the incidence of light was due to the change of polarization in the reflection at the absorption-band edge. The idea of surface colors was succeeded by Michelson,<sup>[4]</sup> who concluded from experiments on reflectivity and its phase change that most metallic samples resembled the surface reflection from a very thin surface layer involving dyes.

In 1917, Lord Rayleigh derived a formula to express the reflection properties from a regularly stratified medium using electromagnetic theory, and considered it as the origin of the colors of certain crystals, of old decomposed glass, and probably of some beetles and butterflies.<sup>[5]</sup> He overviewed the studies of structural colors performed so far,<sup>[6]</sup> and he proposed that the brilliant colors of hummingbirds, butterflies, and beetles, which varied greatly with the incidence of light, were not due to the ordinary operation of dyes but came from the “structural colors”, which were known in thin layers such as soap bubbles. He denied the existence of surface colors and strongly suggested multilayer interference. His son also insisted on multilayer interference from experiments on iridescent beetles.<sup>[7]</sup> Onslow, on the other hand, observed more than 50 iridescent animals using a microscope to settle the conflict between structural colors and surface colors from an experimental standpoint.<sup>[8]</sup> Merritt measured the reflection spectra of tempered steel and *Morpho* butterfly, and interpreted the results in terms of thin-layer interference.<sup>[9]</sup> Mason conducted minute investigations on various types of structural color using a microscope and supported the interference theory.<sup>[10–13]</sup> Thus, the interference of light became the mainstream of the discussion, which finally kept away the interest of physicists.

A complete understanding of these structures was achieved after the invention of the electron microscope. Many biologists attempted to elucidate the structures causing iridescence and

[a] Prof. S. Kinoshita, Dr. S. Yoshioka  
Graduate School of Frontier Biosciences, Osaka University  
Yamadaoka 1–3, Suita, Osaka 565-0871 (Japan)  
Fax: (+81) 6-6879-4600  
E-mail: skino@fbs.osaka-u.ac.jp

accumulated an enormous amount of data. However, the physical interpretation of structural colors had not proceeded since Lord Rayleigh proposed multilayer interference. Only recently have structural colors been the subject of extensive studies, because their applications have rapidly progressed in many fields related to vision such as the paint, automobile, cosmetics, and textile industries.

Nowadays, most of the structural colors in nature are considered to originate from the following five fundamental optical processes and their combinations: 1) thin-film interference, 2) multilayer interference, 3) a diffraction grating effect, 4) photonic crystals, and 5) light scattering. Herein, we will first describe the principle of thin-layer interference, the most common cause of the structure color, and then will explain the structural colors distributed widely in nature from the view-

point of regularity and irregularity of the structure. Finally, we will propose a general principle of structural colors in the natural world and will show their up-to-date applications in various industries.

## 2. Fundamental Optical Processes Related to Structural Colors

### 2.1. Thin-Film Interference

Thin-film interference is one of the simplest structural colors and is widely distributed in nature. Consider a plane wave of light that is incident on a thin layer of thickness  $d$  and refractive index  $n_b$  at the angle of refraction  $\theta_b$  (Figure 1). Then the reflected light beams from the two interfaces interfere with

Shuichi Kinoshita studied physical chemistry at the University of Tokyo, where he obtained a PhD in X-ray photoelectron spectroscopy (1977). Afterwards, he moved to the Osaka University (Department of Physics) and started working on laser spectroscopy of various materials (from gases to lymphocytes). He was particularly interested in studying resonance Raman scattering, fluorescence, and excited-state dynamics appearing as dynamic Stokes shift and transient-hole burning. From 1989 to 1992 he worked at the Hokkaido University on phase-transition phenomena using stimulated light scattering. In 1995 he became professor of physics of the Osaka University, and in 2002 he moved to the newly founded Graduate School of Frontier Biosciences. He has been studying structural colors since 1996; his other research fields include linear and non-linear laser spectroscopy, and pattern formation in nonequilibrium systems.



Shinya Yoshioka studied physics at the Hokkaido University where he received a PhD in femtosecond time-resolved laser spectroscopy (1998). As a postdoctoral fellow at the Venture Business Laboratory of the Osaka University (1998) and a research fellow of the Japanese Promotion of Science (1999), he studied the low-frequency response of molecular liquids. From 2000 to 2001 he was a research associate at the Graduate School of Science of the Osaka University. In 2002 he moved to the newly founded Graduate School of Frontier Biosciences. He is interested in understanding the structural colors in nature and is mainly dedicated to studying butterflies and beetles, from the viewpoint of optical physics, using laser spectroscopic techniques.

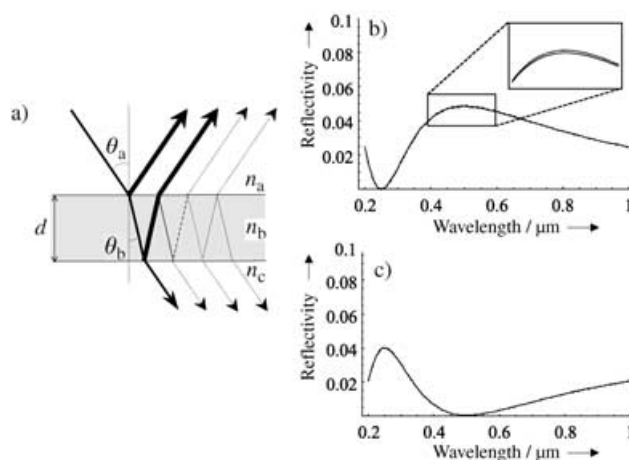


**Figure 1.** a) Configuration of thin-film interference. b,c) Reflectivity from a thin film ( $n = 1.25$ ) with a thickness of  $0.1 \mu\text{m}$  b) in air and c) attached to a material with a higher refractive index ( $n = 1.5$ ). Solid and dashed lines are the calculated curves using an approximate and exact formula, respectively (see text).

each other. In general, the condition of interference differs whether the thin layer is or is not attached to a material having a higher refractive index. The former is the case for antireflective coatings on glass, while a typical example of the latter is a soap bubble. The condition of interference for light with wavelength  $\lambda$ , under which the reflection is enforced (constructive interference), becomes [Eq. (1)]:

$$2n_b d \cos \theta_b = m\lambda \quad (1)$$

where  $m$  is an integer for antireflective coatings, while it is a half integer for the soap-bubble case. Typical examples of the calculations for both cases are shown in Figure 1. It is clear that the reflectivity is relatively low and changes smoothly with wavelength. Thus, the thin-film interference shows only weak dependence on the wavelength. It is easily understood from Equation (1) that the wavelength showing a maximum reflectivity changes continuously to a shorter wavelength as the incident angle is increased. Thus, one of the characteristics of

structural colors, that the color changes with viewing angle, is reproduced.

In thin-film interference, we usually consider only single reflections at each interface. However, with increasing reflectivity at an interface, multiple reflections should be important. The rigorous reflectivity in amplitude is given by Equation (2):

$$r = r_{ab} + \kappa t_{ab} r_{bc} t_{ba} e^{i\phi} \quad (2)$$

where  $\kappa = 1/(1 - r_{bc} r_{ba} e^{i\phi})$  and  $\phi = 4\pi n_b d \cos\theta_b / \lambda$ .  $r_{ab}$  and  $t_{ab}$  are the amplitude reflectivity and transmittance at an interface from a to b, respectively, and are obtained from Fresnel's law. The (power) reflectivity is obtained as  $R = |r|^2$ . Thus, the thin-film interference is converted to the interference in a Fabry–Perot interferometer, the interfaces of which are usually covered with metal or a multilayer coating. Typical examples calculated for the case are shown in Figures 1 and 2. It is clear that at low reflectivity, the modification of the formula on the reflectivity is negligibly small, while at high reflectivity, the reflection spectrum shows periodic dips, where Equation (1) is applied for the destructive interference, as in a Fabry–Perot interferometer.

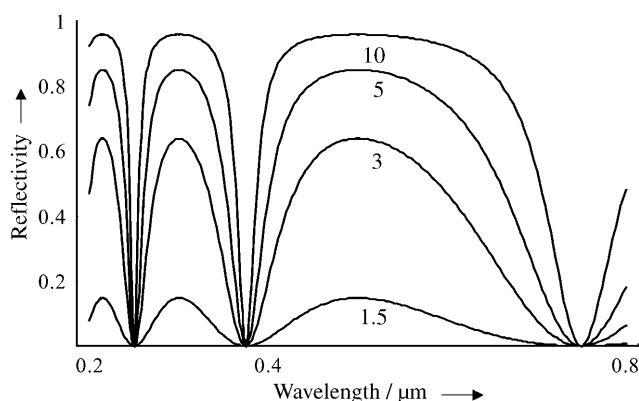


**Figure 2.** Reflectivity from a thin film of thickness  $0.125 \mu\text{m}$  in air under normal incidence. The refractive index of the film is set to be 1.5, 3, 5, and 10.

## 2.2. Multilayer Interference

Multilayer interference is qualitatively understood as the case where a pair of thin layers piles up periodically. Consider two layers designated as A and B with thicknesses  $d_A$  and  $d_B$  and refractive indices  $n_A$  and  $n_B$ , respectively (Figure 3). We assume  $n_A > n_B$  for the present. If we consider a particular pair of layers, the phases of the reflected light both at the upper and lower interfaces between B and A change by  $180^\circ$ . Thus, the relation of an antireflective coating, as in thin-film interference, can be applied as [Eq. (3)]:

$$2(n_A d_A \cos\theta_A + n_B d_B \cos\theta_B) = m\lambda \quad (3)$$

for constructive interference, with the angles of refraction in layers A and B as  $\theta_A$  and  $\theta_B$ , respectively.

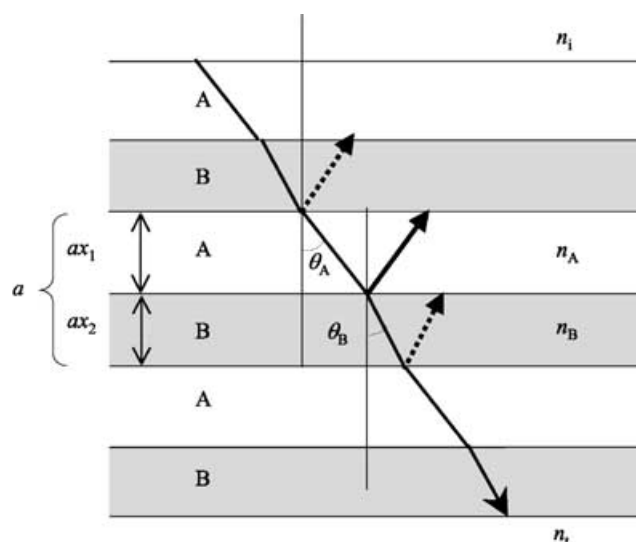


**Figure 3.** Configuration of the interference from a multilayer consisting of layers A and B with a thickness of  $ax_1$  and  $ax_2$  and a refractive index of  $n_A$  and  $n_B$ , respectively.  $n_i$  and  $n_t$  are the refractive indices of the incident and transmitting spaces. The dashed arrows indicate the reflected light subject to a phase change of  $180^\circ$ .

On the other hand, the phase of the reflected light does not change at an A–B interface. Thus, if a soap-bubble relation of Equation (1) [Eq. (4)]:

$$2n_A d_A \cos\theta_A = (m' + \frac{1}{2})\lambda \quad (4)$$

is further satisfied, the reflection from this interface adds to the above interference and the multilayer should give the maximum reflectivity, where  $m' < m$  would be satisfied because of the restriction of the thickness. In particular, Equations (3) and (4) for  $m = 1$  and  $m' = 0$  correspond to the case where the optical path lengths, defined as the length multiplied by the refractive index, for layers A and B are equal to each other. Land called this case an “ideal multilayer”.<sup>[14]</sup> However, if the thickness of layer A does not satisfy Equation (4), while the sum of layers A and B satisfies Equation (3), the reflection at the A–B interface works destructively and the peak reflectivity may decrease. This case corresponds to a “nonideal multilayer”.

The calculation of the reflectivity from the multilayer has been fully described since Lord Rayleigh presented his paper in 1917.<sup>[5]</sup> Nowadays, the reflectivity and transmittance are usually calculated through a transfer matrix method. This method is suitable for the evaluation of structural colors, because it is applicable to multilayers having arbitrary refractive indices and thickness without any periodicity. Since the detail of the method has been described in the literature,<sup>[14–16]</sup> here we will show only the calculated results.

Figure 4a shows the reflectivity for an ideal multilayer with a varying number of layers under normal incidence. This figure corresponds to the cases where the difference in the refractive indices between the two layers is very small, which is a typical case for polymer materials. With increasing number of layers,

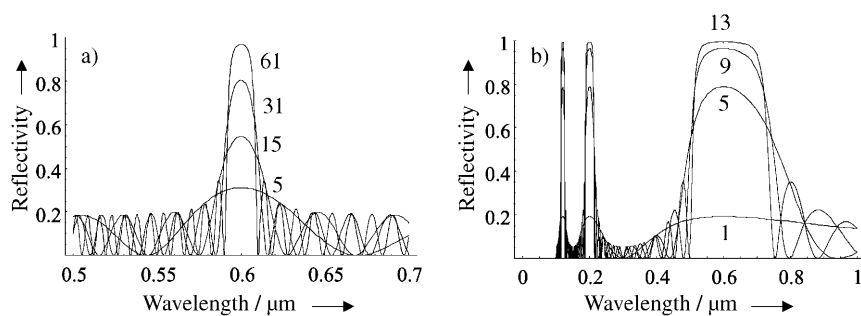


**Figure 4.** Reflectivity from a multilayer with various numbers of layers. a) The difference of the refractive indices for the two layers is small;  $n_A=1.55$  and  $n_B=1.60$ . b) A large refractive index difference;  $n_A=1.6$  and  $n_B=1.0$ . The thickness of each layer is set to satisfy an ideal multilayer and the total optical path length of the sum of layers A and B is set to  $0.25 \mu\text{m}$ .

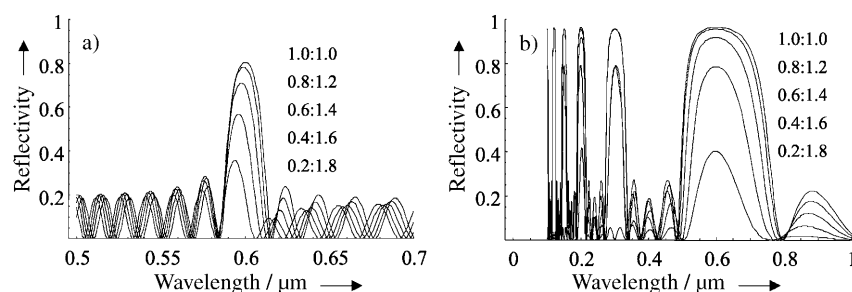
the reflectivity increases rapidly, while its bandwidth decreases remarkably. It is also noticed that an oscillation of the reflectivity of 0–20% is present in the background. This is because the difference between the refractive indices of air and the material is much larger than the interlayer difference. Thus, the multilayer behaves like a thin film.

Figure 4b shows the reflection spectrum of the multilayer with a large difference in the refractive indices of 0.6. When the difference of the refractive indices of the two layers becomes large, the maximum reflectivity reaches unity only with several layers. For an ideal multilayer under normal incidence, the maximum reflectivity occurs around the wavelengths where the relation  $2n_A d_A = 2n_B d_B = (m + 1/2)\lambda$  is satisfied. The amplitude reflectivity at this wavelength is calculated as  $r = (1-p)/(1+p)$ , where  $p$  satisfies the relations  $p = (n_t/n_i)(n_B/n_A)^N$  and  $p = (n_A^2/n_i n_t)(n_A/n_B)^N$ , in which the total number of layers  $N$  takes an even and odd number, respectively. Here we put the refractive indices of the incident and transmitting spaces as  $n_i$  and  $n_t$ . On the contrary, for the wavelength at which  $m$  is a half integer, the reflection from A–B and B–A interfaces interferes destructively. The reflectivity at this wavelength becomes  $r = (n_i - n_t)/(-n_i + n_t)$  and is null when the refractive indices of the incident and transmitting regions are the same. We can see this effect in Figure 4b, where the reflectivity at the wavelengths of  $1/2, 1/4, 1/6, \dots$  of the main wavelength becomes zero, while those of  $1/3, 1/5, 1/7, \dots$  form a peak.<sup>[14]</sup>

Next, we will briefly mention the result for a nonideal multilayer. Figures 5a and 5b show the calculated results corresponding to Figures 4a and 4b, in which the ratio of the optical path length of layer A with a higher refractive index decreases, while the sum of the optical path lengths is kept constant. Figure 5a shows the result for a small difference in the refractive indices. The peak reflectivity decreases with increas-

ing asymmetry, while the bandwidth slightly decreases. At the same time, the peak position shifts toward shorter wavelengths. Figure 5b shows the result for a large difference in the refractive indices. The deviation from the ideal multilayer becomes remarkable, that is, both the peak reflectivity and the bandwidth decrease with increasing asymmetry. It is also noticed that the reflectivity at a wavelength of  $1/2, 1/4, 1/6, \dots$  of the main wavelength restores quickly.

Equations (3) and (4) are, however, too simple to express the essential features of the multilayer interference. In fact, they are only applicable to the case where the difference in the re-



**Figure 5.** Reflectivity from a nonideal multilayer corresponding to Figure 4. a) A small difference in the refractive index and b) a large difference. The total optical path length is set to take a constant value of  $0.25 \mu\text{m}$ , while the ratio of the optical path lengths for layers A and B is varied as indicated in the figure.

fractive indices of the two layers is sufficiently small. Otherwise, the multiple reflections modify the interference condition to a large extent. Details on this point are discussed in conjunction with recent studies on photonic crystals. Namely, the system with an infinite number of layers is the simplest case of a one-dimensional photonic crystal, in which the dielectric constant is periodically modulated. Here, we will consider only the first reflection band, that is,  $k \approx \pi/a$  and  $\omega \approx b_0 k / \sqrt{\mu_0}$ , with  $a$  and  $\mu_0$  the period of the multilayer and the permeability of the vacuum, respectively.  $b_j$  is the expansion coefficient of the reciprocal of the dielectric constant with respect to the reciprocal lattice vector and is given below. After complicated calculations, we finally obtain the approximate expression for the dispersion relation near the first bandgap as [Eq. (5)].<sup>[17]</sup>

$$\omega_{\pm}(h) \approx \frac{\pi}{a\sqrt{\mu_0}} \sqrt{b_0 \pm |b_1|} + \frac{a}{2\pi\sqrt{\mu_0}\sqrt{b_0 \pm |b_1|}} \left( b_0 \pm \frac{2b_0^2 - |b_1|^2}{|b_1|} \right) h^2 \quad (5)$$

where  $h \equiv k - \pi/a$ . A schematic diagram for the dispersion relation of a one-dimensional photonic crystal is shown in Fig-

ure 6a. The bandgap just corresponds to the high-reflection band, whose band center and bandwidth correspond to  $\omega_c = \pi\sqrt{b_0 \pm |b_1|}/(a\sqrt{\mu_0})$  and  $\Delta\omega = \omega_+ - \omega_-$ , respectively. For

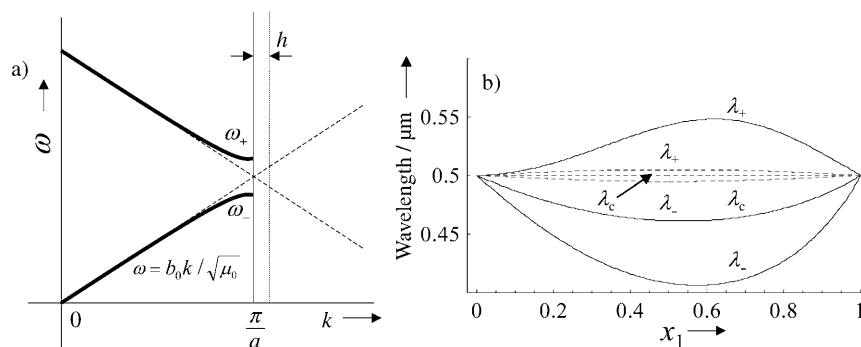


**Figure 6.** a) Schematic illustration of the dispersion curve near the first bandgap and b) upper and lower edges of a one-dimensional photonic bandgap for the small difference in the dielectric constant of  $\varepsilon_1 = 1.55^2$  and  $\varepsilon_2 = 1.60^2$  (-----), and for the large difference of  $\varepsilon_1 = 1.60^2$  and  $\varepsilon_2 = 1.00^2$  (—). The optical path length of the sum of the two layers is  $0.25 \mu\text{m}$ .

periodic double layers whose dielectric constants are expressed as  $\varepsilon_1 = n_1^2$  and  $\varepsilon_2 = n_2^2$ , the band center in a wavelength unit  $\lambda_c$  is expressed as Equation (6):

$$\lambda_c = 2a / \sqrt{\frac{1}{n_2^2} \left\{ 1 + \frac{n_2^2 - n_1^2}{n_1^2} x_1 \right\}} \quad (6)$$

where we put  $b_0 = (x_1/n_1^2) + (x_2/n_2^2)$  and  $|b_1| = \sin(\pi x_1)(n_1^{-2} - n_2^{-2})/\pi$  with  $x_1$  and  $x_2$  as the ratios of the thickness of the layers 1 and 2 to their sum. When  $n_1 \approx n_2$ , this reduces to  $\lambda_c \approx 2a(n_1 x_1 + n_2 x_2)$ , which corresponds to Equation (3). Figure 6b shows the calculated results of  $\lambda_c$  and  $\lambda_{\pm}$  ( $\equiv 2\pi/\omega_{\mp}(0)$ ) for small and large differences in the refractive indices between the two layers. It is clear that the bandwidth in the large difference in the refractive index is much larger than that in the small difference. Moreover, it is found that the deviation of the band center from Equation (3) becomes remarkable. In the following sections, the reader will soon understand that the fundamental optical processes, such as interference, diffraction, and scattering of light, are complicatedly connected with various structures to generate unique structural colors in nature.

### 3. Structural Colors in *Morpho* Butterflies

#### 3.1. Historical Review

*Morpho* butterflies bearing brilliant blue color in their wings are the most suitable creatures to explain the complicated features of the structural colors in nature, and also to understand the importance of the regularity and irregularity in their colors. *Morpho* species live exclusively in Central and South America, and their males are especially brilliant. We show typical examples in Figure 7. So far, 50–80 species are classified into genus *Morpho*, although the systematic classification is still in progress.<sup>[18]</sup>

About 120 years ago, Walter<sup>[3,6]</sup> reported the observation of the scales of *M. menelaus*, which strongly glittered green-blue in air, became purely green and shining less strongly in ether

( $n = 1.36$ ), yellowish green and weakly shining in chloroform ( $n = 1.45$ ), and only perceptibly yellow-green under direct sunshine in a dark room when immersed in benzene ( $n = 1.52$ ) or carbon disulfide ( $n = 1.64$ ). Walter ascribed this phenomenon to the effect of dyes in chitin, whose refractive index is coincident with that of benzene or carbon disulfide. Michelson<sup>[4]</sup> measured the phase change in the reflection from the blue wing of *M. aega* under normal incidence and found that it changed with the orientation of the wing. He attributed this

change to the diffraction of light by many hairs growing on the wing, and concluded that the essential cause of the blue color was the “surface color”.

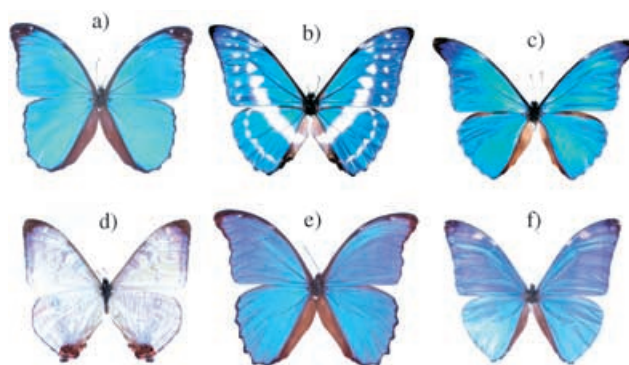


**Figure 7.** *Morpho* butterflies. a) *M. menelaus* (wingspan = 110 mm), b) *M. cyprius* (120 mm), c) *M. rhetenor* (120 mm), d) *M. sulkowskyi* (85 mm), e) *M. didius* (155 mm), and f) *M. adonis* (95 mm) [photographed by Okamoto].

Lord Rayleigh,<sup>[5,6]</sup> on the other hand, strongly suggested the possibility of multilayer interference in brilliant colors. Onslow<sup>[8]</sup> investigated the scales of *M. menelaus* and found that two layers of scales were combined to form the brilliant greenish blue. The lower scale had periodic chitin plates  $0.85\text{--}0.9 \mu\text{m}$  apart, each of which was transparent and prolonged as compared with the noniridescent scale. However, the separation of the plates he observed was too long to ascribe it to any interference phenomenon. More thorough investigation was made by Mason,<sup>[12]</sup> who investigated the scales of *M. menelaus* and found that the scale was constituted by many vanes and that a single vane itself was responsible for the brilliant reflection. He also found that the reflected plane was not parallel to the plane of the scale. He compared the optical properties with thin-layer interference and found a resemblance. In his paper,

a surprisingly accurate illustration of a *Morpho* scale was inserted (Figure 8a).

The structural analysis of the *Morpho* scale was finally concluded after the invention of the electron microscope. Anderson and Richards<sup>[19]</sup> first observed the electron microscopic images of a scale of *M. cypris* and reported that it consisted of hundreds of elaborate vanes possessing linear thickenings 0.2  $\mu\text{m}$  apart, which reinforced the reflection of blue light (Figure 8b). Furthermore, chemical tests showed that the scale was not composed of chitin, but of the "principal component of the external parts of most insects", that is, cuticle. Later, Ghiradella<sup>[20–24]</sup> investigated various types of lepidopteran scales using an electron microscope and classified the structural colors according to their positions located on the scale. In her classification, the scales of *Morpho* butterflies were categorized into "ridge-lamella" types. She also performed a developmental investigation of the scale.<sup>[22,25,26]</sup>

Contrary to the structural and biological development of the studies on the *Morpho* butterflies, the physical interpretation of their structural colors did not progress much after the establishment of the multilayer interference hypothesis in the 1920s. However, the requirements for structural colors as display materials increased rapidly in the 1990s in various industries such as paint, automobile, textiles, and cosmetics, which has invoked the study of *Morpho* butterflies again from a physical standpoint. In this trend, Tabata et al.<sup>[27]</sup> performed the chemical and optical analysis of the wing of *M. sulkowskyi* and *M. adonis*. They measured the angle- and wavelength-resolved reflectance of the wing, and analyzed the results by a multilayer interference theory. On the other hand, Vukusic et al.<sup>[28]</sup> performed a sophisticated measurement on scales of *M. rhetenor* and *M. didius*. They investigated, for the first time, the angular dispersion of the transmitted and reflected light from a single scale of *M. rhetenor* in air and in isopropyl alcohol ( $n=1.38$ ) or bromoform ( $n=1.58$ ). They also measured a cover and ground scale of *M. didius* and found that the transmitted light showed clear diffraction spots corresponding to periodically separated ridges, while the reflected light showed broad angular dependence, although that from a scale of *M. rhetenor* was split into two. They determined the absolute reflectivity from a single scale for various wavelengths and explained it using a multilayer interference theory.

### 3.2. Physical Interpretation of Blue Coloring

We believe that the blue coloring of *Morpho* butterflies is explainable in terms of the combined action of interference and diffraction of light coupled with pigmentation.<sup>[29,30]</sup> In this Section, we will briefly explain its physical mechanism along with the observations described above. For the time being, we choose *M. didius* as an example, a typical *Morpho* species with large blue wings. At first, it is easily noticed that the observation of the color change, when the viewing or incident angle is changed and also when the wing is immersed in liquid with a high refractive index, cannot be explained simply in terms of pigmentation.

More detailed observation of the wing reveals that the change of the blue color into violet is observable only when the viewing angle approaches the plane of the wing under normal incidence, and also in cases where we move our eyes perpendicularly to the longer side of the scale. Thus, the blue persists in a large angular range in this direction. On the other hand, when we move parallel to the longer side of the scale, the reflection is found to cease rather quickly, which implies that the reflection occurs only in a small angular range. Thus, strong blue reflection with a diffusive and anisotropic nature is characteristic of the *Morpho* wing.

Optical and electron microscopic observations demonstrate that the wing of *M. didius* has two types of scales, cover and ground scales, both on the fore and hind wings (Figure 9). In most of the *Morpho* species, the ground scales are mainly responsible for the structural color except for a few species such as *M. adonis*, where the cover scales seem to play a central role. The cover scale in most species shows a unique size and changes from species to species, which implies the presence of its specific function. Both scales have many equidistant ridges along the long side of the scale, each of which shows brilliant blue color under high magnification. A typical separation of the ridges is about 1  $\mu\text{m}$ .

It is possible to consider that the regularly arranged ridges would work as a diffraction grating. However, as Vukusic et al.<sup>[28]</sup> showed in a single-scale transmission and reflection study, and also as shown in Figure 10, the diffraction spots are only visible in the transmission side, and not in the reflection side. This finding suggests that the spacing between ridges

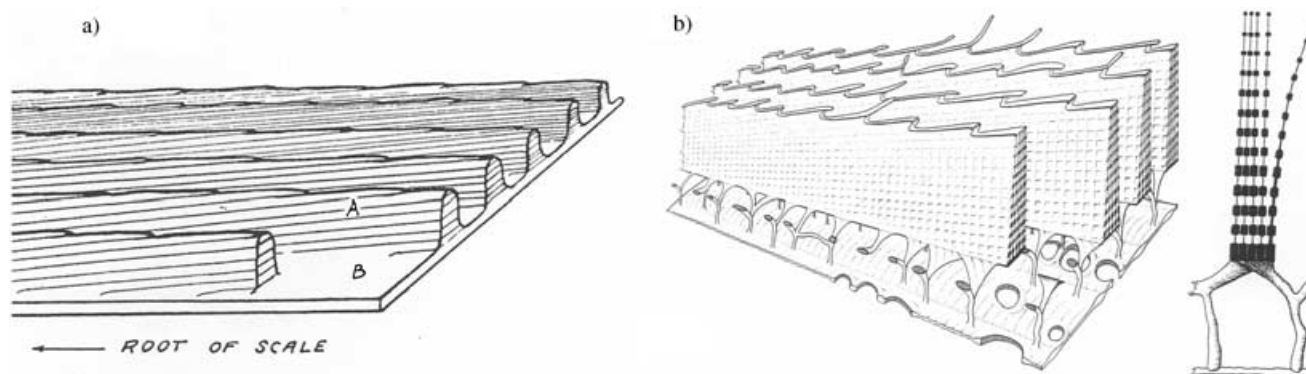
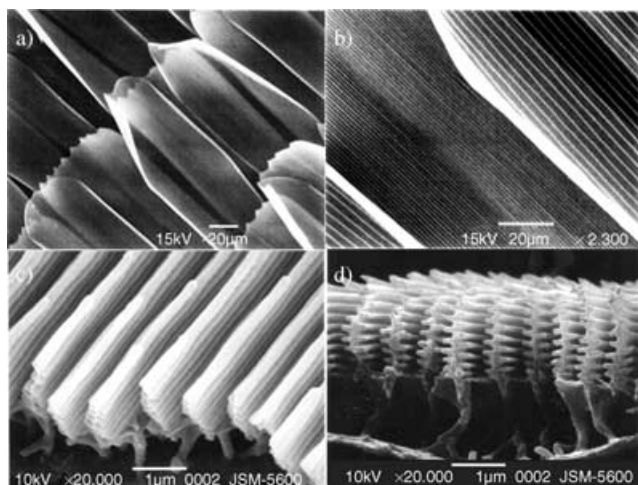
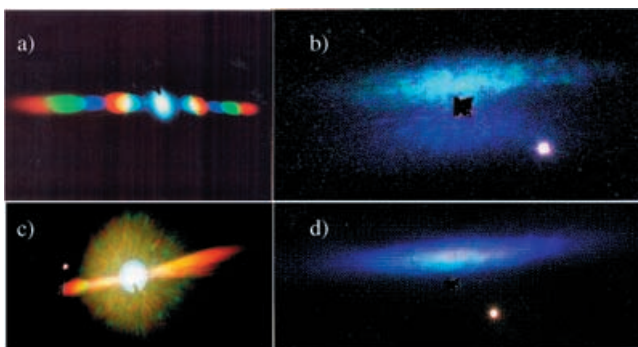


Figure 8. Illustrations given by a) Mason (1927) for a scale of *M. menelaus*,<sup>[12]</sup> and b) Anderson and Richards, Jr. (1942) for a scale of *M. cypris*.<sup>[19]</sup>



**Figure 9.** Scanning electron microscopic images of a,b) cover and ground scales of *M. didius*, and c,d) cross-sections of its ground scale.<sup>[29,30]</sup> The bars are a) 20, b) 10, c) 1, and d) 1  $\mu\text{m}$ .



**Figure 10.** a,c) Transmission and b,d) reflection patterns obtained under the illumination of white light on a,b) a cover scale and c,d) a ground scale of *M. didius*.<sup>[29,31]</sup>

works as a diffraction grating, but the ridges themselves do not. This implication is quite important to understand the essential features of the structural color in this butterfly.

Electron microscopic observation under high magnification clarifies that the lamellar structure consisting of alternate layers of cuticle and air is present in each ridge (Figure 11) and, moreover, the cuticle layer runs obliquely with respect to the plane of the scale shown in Figure 9c. An oblique view of the ridges shows that the upper ends of the cuticle layers are distributed randomly over a whole area of the scale.<sup>[30]</sup> Thus, the heights of the ridges are not so regular in an optical sense and are distributed within a layer interval of 0.2  $\mu\text{m}$ . If this is true, the light diffracted at each ridge is randomly superimposed and no interference should occur. In other words, the properties of interference and diffraction are essentially determined by those of a *single* ridge. It is easily verified, from spatial Fourier analysis of the cross-section of the ridge, that the split of the reflection pattern<sup>[28]</sup> observed in a scale of *M. rhetenor* results from the antisymmetric lamellar structure with respect to the pillar of the ridge.

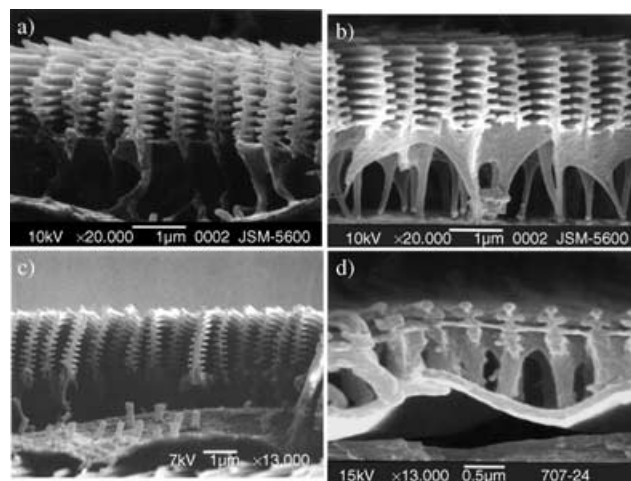


**Figure 11.** Scanning electron microscopic images for the cross-sections of ground scales of a) *M. didius*, b) *M. sulkowskyi*, and c) *M. rhetenor*, and for a cover scale of d) *M. adonis*.<sup>[30]</sup> The bars are a–c) 1 and d) 0.5  $\mu\text{m}$ .

The physical importance of this elaborate structure is clear. The lamellar structure within a ridge works as an element of quasi-multilayer interference, while the narrow width of ridges with different heights causes light diffraction without interference among neighboring ridges. (Here we call the interference in the *Morpho* wing quasi-multilayer interference, because the width of the layer is so small that the multiple reflection at each layer does not occur eventually owing to the diffraction effect.) The large difference in the refractive indices between cuticle ( $n=1.56$ <sup>[28]</sup>) and air ( $n=1$ ), and the layer thickness nearly satisfying an ideal multilayer, cause the high reflectivity with a large bandwidth. Thus, the *Morpho* butterfly realizes simultaneously the high reflectivity in a wide wavelength range and the generation of diffusive light in a wide angular range. At a glance, these two characteristics seem to contradict each other in the usual optical sense. However, the *Morpho* butterfly realizes these seemingly conflicting requirements by combining appropriate amounts of regularity and irregularity.

The mystery of the *Morpho* wing does not end at the above conclusion. Although the microscopic ridge–lamella structures are essentially the same for the two *Morpho* butterflies *M. didius* and *M. sulkowskyi*, as shown in Figures 11 a and 11 b, these wing colors are completely different, that is, *M. didius* displays a deep-blue wing without gloss, while *M. sulkowskyi* has a pearly white, glossy wing. The difference in the optical responses of these species are well illustrated by the transmission/reflection properties of the wing.<sup>[30]</sup> Figure 12 shows the results for the wings of various *Morpho* species. In this figure, the optical response of the wing under normal incidence is divided into transmission, reflection, and the rest connected with the absorption due to intrinsic pigment. It is immediately evident that the wing of *M. sulkowskyi* almost has a lack of absorption. However, considering that the light perceptible to the eye is only the reflected part, one will notice that the reflectivity at the peak wavelength is rather higher in *M. sulkowskyi* than that in the others. The remarkable difference, in reality, is the reflectivity near a complementary color to blue

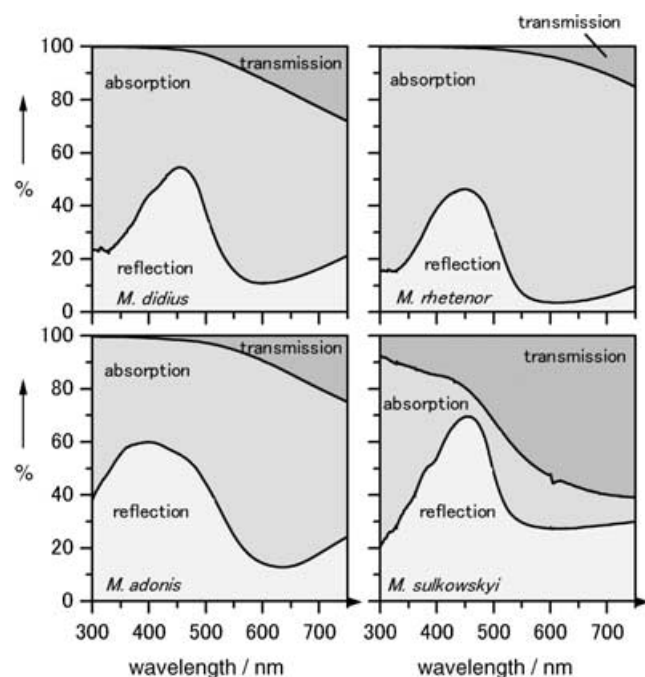


Figure 12. Transmission, absorption, and reflection properties of the wings of *M. didius*, *M. rhetenor*, *M. adonis*, and *M. sulkowskyi*.<sup>[30]</sup>

around 600 nm. *M. sulkowskyi* shows an extraordinarily high reflectivity of 30%, while the others have a 5–15% reflectivity. Particularly, *M. rhetenor*, which displays the most brilliant blue wing, shows very low reflectivity. Thus, the presence of the pigment enhances the contrast of blue coloring by absorbing the unwanted complementary color.

Another important role of the pigment is the change of hue by adding light scattered at the membrane and ventral scales to the reflection without the cost of changing the microscopic structure. The *Morpho* butterfly seems to have an intention to use this effect to add white spots on the dorsal side of the blue wing in *M. cypris*, because white spots are also placed at the corresponding ventral side of the wing regardless of whether the original wing pattern is disturbed.

Finally, the role of cover scales has recently been investigated by us.<sup>[31]</sup> The essential property of the cover scale is characterized by its structure. The cover scale consists of well-separated ridges with lamellar structure and of membranes between them. These two elements behave as independent origins of the structural color of quasi-multilayer interference in the former and thin-film interference in the latter. Surprisingly, the reflectivities of these two elements show essentially the same peak wavelength of 470 nm, although their mechanisms are completely different. Further, owing to the obliquely running lamella, the directions of the reflection differ by 16° from the thin-film interference, with almost the equivalent contribution to the total reflectivity. Thus, the cover scale plays the role of a wavelength-selective optical diffuser. Since, without cover scales, a glossy blue color comes out owing to the highly reflective ground scale, the cover scale simultaneously plays the role of an adjuster for the gloss of the wing.

In summary, the elaborate structure together with the pigmentation displays quite a few optical phenomena within the wing of the *Morpho* butterfly, as shown in Figure 13: 1) high reflectivity in the blue region due to quasi-multilayer inter-

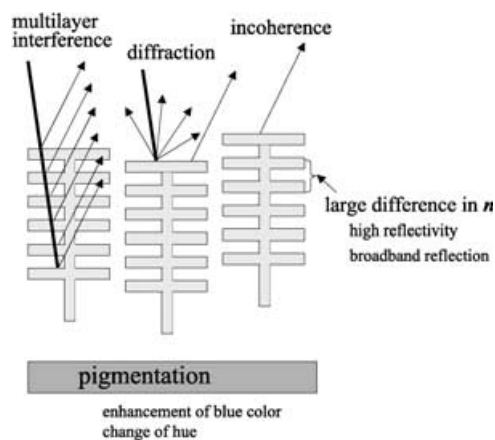


Figure 13. Principles of blue coloring in the *Morpho* butterfly.

ence, 2) diffusive reflection due to the narrow width and the irregular height of a ridge, 3) pigmentation to enhance the blue contrast or to change the hue without the cost of the structure, and 4) gloss of the wing controlled by covering transparent scales as an optical diffuser. Thus, the cooperation of regularity and irregularity, and the collaboration of the structural color with pigmentation constitute a central part of the *Morpho* color. We think these two aspects are fundamental to understanding structural colors in nature. In the following, we will inspect structural colors from these standpoints.

## 4. Thin-Layer Interference in Structural Colors

### 4.1. Multilayer Interference

Structural colors related to multilayer interference are most commonly found in nature, while thin-film interference is only used in a subsidiary manner, probably because both reflectivity and selectivity of wavelength are generally low. Metallic reflection from the elytra of beetles is one of the most well-known examples of multilayer interference.<sup>[8,12,32–34]</sup> Figure 14 shows photographs of the Japanese jewel beetle, *Chrysochroa fulgidissima*, which can be collected around its larval food plant, hackberry, owing to its glittering. The change in viewing angle from the normal to the elytron to its tail reveals a remarkable color change from yellowish green to deep blue, while on the ventral side, the color changes from reddish brown to green. The change is rather continuous, which differs from the case of the *Morpho* butterfly. Thus, the characteristics of thin-layer interference are clearly observed in the dependence on viewing angle. Under a microscope of high magnification, the elytron is covered with a minute pattern of about 10 μm all around, which is more easily seen by a scanning electron microscope (Figure 15b). The pattern is expressed by an ensemble of pen-



**Figure 14.** Dorsal and ventral views of the Japanese jewel beetle (body length = 40 mm), *Chrysochroa fulgidissima*, at various viewing angles.<sup>[34]</sup>

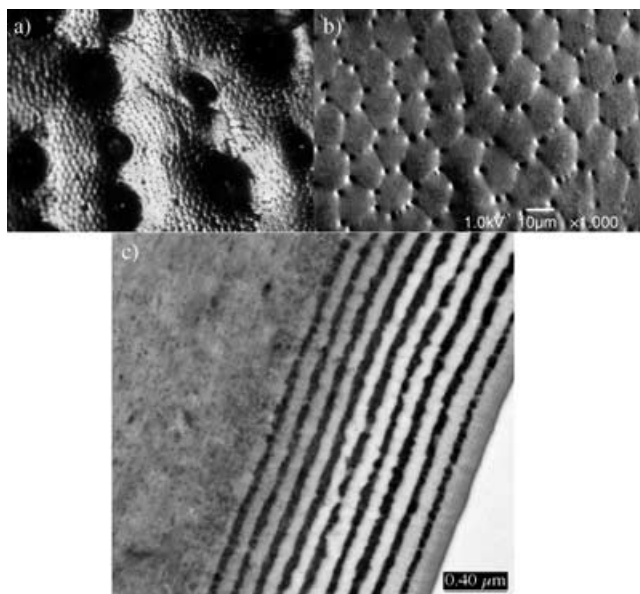


**Figure 15.** Surface of an iridescent elytron of a Japanese jewel beetle, *Chrysochroa fulgidissima*, observed under a) an optical microscope and b) a scanning electron microscope (bar = 10  $\mu\text{m}$ ), and c) its cross-section observed under a transmission electron microscope (bar = 0.40  $\mu\text{m}$ )<sup>[34]</sup> [courtesy of Prof. Hariyama].

tagons or hexagons with a hole at each apex. The orientation of a plane including each polygon is distributed slightly as if they destroy the flatness of the plane.

Kurachi et al.<sup>[33]</sup> investigated the cross-sections of the elytra of various beetles using a transmission electron microscope and found that they consisted of epicuticle in the outer side and exocuticle in the inner side. In the case of a leaf beetle, *Plateumaris sericea*, the thickness of each region is 0.3–0.5 and 10  $\mu\text{m}$ , respectively. The epicuticle consists of five alternate layers, the total thickness of which depends on the apparent

color of the elytron and changes from blackish blue to red. The authors examined the reflection spectra of these species and found that refractive indices of 1.4 and 1.7 for these two layers reproduced the color fairly well. They also observed the elytron of the jewel beetle and 20 alternate layers were present in the epicuticle region.<sup>[35]</sup> Analysis by the multilayer interference theory with the refractive indices of 1.5 and 1.7 again reproduced the reflection spectrum. Thus, the structural color in the jewel beetle comes essentially from multilayer interference. However, it is easily noticed that a simple multilayer model gives only a specular reflection so that the elytron would be mirror-like. A mirror cannot assert its existence, but only reflects the surrounding view. If a creature could assert itself, it should have a device to emit light from itself. The jewel beetle makes this possible by creating many irregular structures on its elytron to destroy the flatness. Thus, the multilayer and the polygon structure play the roles of regularity and irregularity in this insect.

The exocuticle region is known to form a helicoidal structure very similar to that of cholesteric liquid crystals.<sup>[4,33,36]</sup> When the unpolarized white light is incident on this structure, left-circularly polarized light is selectively reflected with the peak wavelength determined by  $np = m\lambda$ , where  $n$ ,  $p$ , and  $m$  are the average refractive index, the pitch of the helicoid, and an integer, respectively. The first observation of circularly polarized light reflected from beetles was reported perhaps by Michelson.<sup>[4]</sup> He examined a gold beetle named *Plusiotis resplendens* and found the circularly polarized reflection under normal incidence. He deduced that the effect was due to a screw structure of a molecular size. Neville proceeded with this work and quantitatively explained the beetles' optical properties by comparison with cholesteric liquid crystals.<sup>[36]</sup> It is now understood that the circularly polarized light originates from lyotropic cholesteric liquid crystals created in an exocuticle region, which is a natural consequence of optically active molecules in creatures. Thus, if the exocuticle region is optically exposed to the surface of the elytron as in the scarabaeid beetle, circular polarization is observed as shown in Figure 16.<sup>[37]</sup> In the case of the jewel beetle and leaf beetle where the epicuticle region consists of a high reflector due to a multilayer, the outer epicuticle mainly contributes to the reflection, which is essentially insensitive to the polarization.

Multilayer structures are widely distributed in animals and even in the plant kingdom,<sup>[38]</sup> although they are not well investigated from a physical viewpoint. Butterflies and moths are

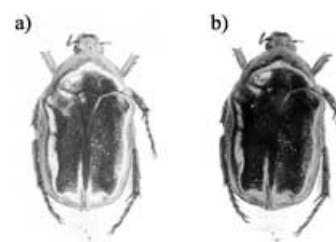


**Figure 16.** Flower beetle (body length = 25 mm), *Prataetia pryri*, observed a) without and b) with a right-circular polarizer.<sup>[37]</sup>

again a treasure of multilayer interference. Mason has already reported a schematic illustration of the scale of a moth of family Uraniidae using an optical microscope.<sup>[12]</sup> The multilayer was located at the lower part of the scales parallel to its plane and 5–15 films were found to be present. This finding was confirmed later by TEM observations made by Lippert and Gentil for *Urania ripheus*,<sup>[39]</sup> and by Ghiradella for *U. fulgens*.<sup>[21]</sup>

Quite an interesting variation of multilayer interference has been recently found in the Indonesian green butterfly, *Papilio palinurus*.<sup>[40]</sup> The green scale of this butterfly shows a wide spacing between ridges, where a regular two-dimensional array of concavities 4–6  $\mu\text{m}$  in diameter and 0.5–3  $\mu\text{m}$  in depth are present (Figure 17). Below a round concavity, a curved multilayer consisting of about 20 alternate layers of cuticle and air is present. When white light is incident on this structure, yellow light hitting directly on the bottom of a concavity is selectively reflected, while blue light hitting the side of the concavity is reflected, hits again on the opposite side of the concavity wall, and is then reflected back in the reverse direction. Thus, only yellow and blue colors are selectively reflected, which produces a green color by color mixing in the eye. Because of the oblique reflection of blue color at the wall of the concavity, a color change with the polarization of light is also observed. In similar *Papilio* butterflies, *P. ulysses*<sup>[40]</sup> and *P. blumei*,<sup>[41]</sup> on the other hand, the concavity is shallow and the usual multilayer reflection such as that in Uraniidae is observed. The diffusivity of light in these butterflies may be realized by their concave layers.

Probably the most exciting multilayer ever reported is that found in tropical fish. Nagaishi and Oshima<sup>[42]</sup> reported the presence of regular layers of very thin guanine crystals of not more than 5-nm thickness in the iridescent cells of *neon tetra* (Figure 18). Each cell contains two rows of parallel platelets and simultaneously changes their inclinations giving rise to an alteration of the distance between the platelets. It is found that light induces a decrease in the distance, while darkness does the reverse. The authors call it the Venetian blind mechanism. The movement of the platelets is considered to be neurally controlled and the tubulin-dynine interactions play a decisive role. Thus, the structural color in this case should be called a *dynamical* one, whose selective color changes according to changes in the environment. On the other hand, its multilayered platelets may be an

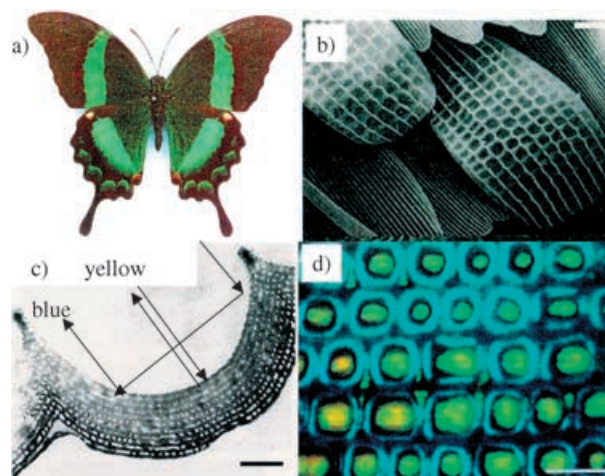


**Figure 17.** Color-mixing mechanism due to concavities in a scale of a) *Papilio palinurus* (wingspan = 100 mm).<sup>[40]</sup> b–d) SEM, TEM, and optical micrographs of the scale, respectively. The bars are b) 5, c) 1, and d) 10  $\mu\text{m}$ .

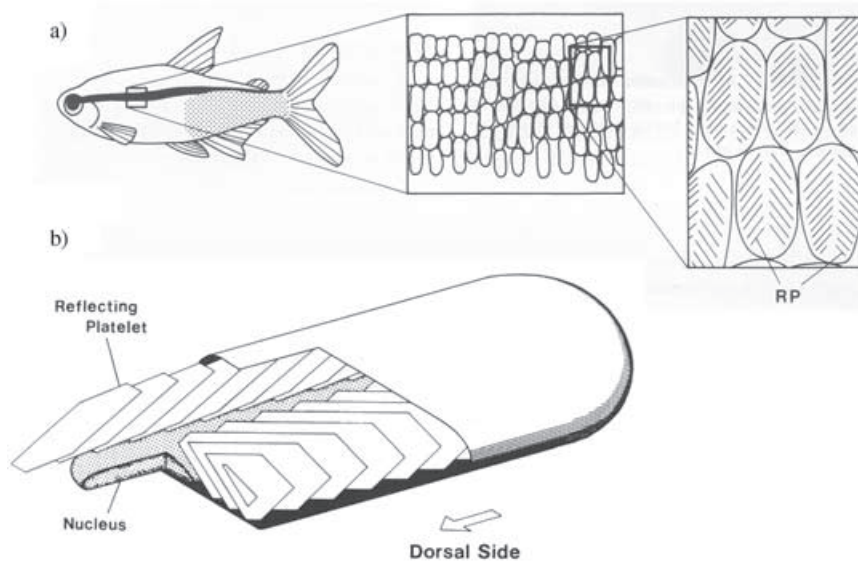


**Figure 18.** a) Iridescent cells under a blue stripe in *neon tetra* (body length = 30 mm). Each cell contains two rows of parallel platelets of guanine crystals as shown in (b), which move like a Venetian blind.<sup>[42]</sup> RP: reflecting platelet.

extremely nonideal multilayer consisting of guanine crystals and cell sap. Nagaishi and Oshima assumed the refractive indices for both layers were 1.83 and 1.37, and simulated the reflectivity. From the features of the nonideal multilayer, the reflectivity is generally low, that is, even when the number of platelets is increased up to ten, the reflectivity becomes only 0.1 with a width of 80 nm. Since these results do not agree well with the reflection spectrum measured experimentally, the

effect of any irregularity such as variations of the distances and of the inclination angles of platelets, and the cooperation of pigmented cells, should be further investigated.

#### 4.2. Reflector and Antireflector

Another important role of the multilayer reflection is the so-called biological reflector,<sup>[6,43–47]</sup> which is commonly distributed in the animal world. Strictly speaking, this may not be classified into structural colors, but is often discussed in this context, because the interaction of light with minute structures plays a decisive role.

Among the butterfly species in Danaidae and Nymphalidae, there exist species showing surprisingly metallic pupae bearing gold or silver colors (Figure 19). These pupae were described

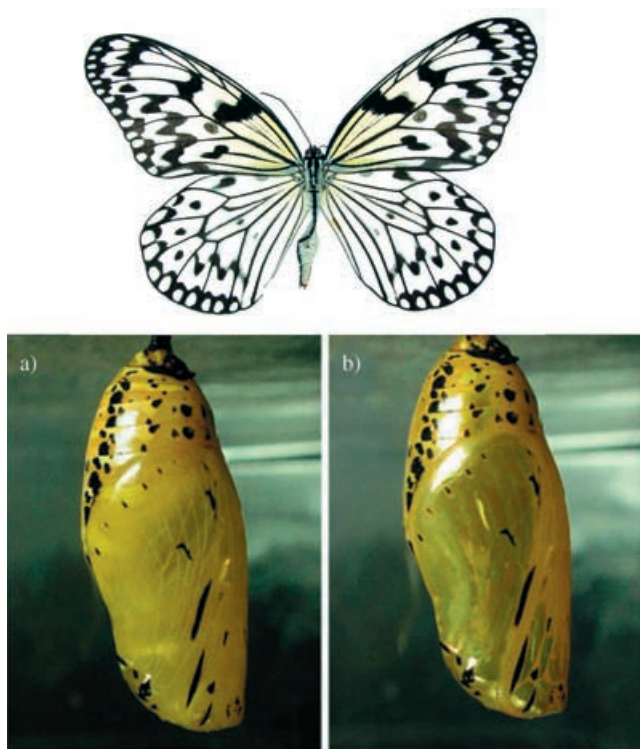


**Figure 19.** Pupa of a tree nymph (wingspan = 120 mm), *Idea leuconoe*, whose color changes from a) yellow to b) gold within two days after pupation [photographed by Fujii].

by Poulton<sup>[43]</sup>, who reported that the metal-like appearance of pupae of *Vanessa urticae* needed the presence of moisture to glitter. Lord Rayleigh<sup>[6]</sup> explained that its possible cause was the interference of light due to a laminated layer under a lower part beneath the surface, which consisted of chitinous lamellae of higher refractive index and liquid of a lower refractive index. Later, Steinbrecht et al.<sup>[44]</sup> performed electron microscopic observations and found that the reflecting cuticle of *Amauris* and *Euplorea* had reflectance exceeding 70% with a mirror quality. The endocuticle layers consisted of 250 pairs of alternating dense and clear layers in the electron microscopic image, and the thickness of the clear layers was systematically

changed, first increasing and then decreasing from outside to inside. Thus, the large number of layers and the change of the layer thickness are responsible for the high reflectivity over a wide wavelength range. It is noticed that the lack of irregularity in this insect makes the multilayer interference mirror-like, which endues the function of camouflage.

Similar types of biological mirrors<sup>[45–47]</sup> were reported frequently. The silvery sheen of the skin and scales of a smelt were thought to be composed of stacks of four to five guanine crystals of area  $25 \times 5 \mu\text{m}^2$  with a thickness of 100 nm ( $n = 1.83$ ). Guanine stacks are also found in the cat's eye, known as a tapetum. In the visual systems of animals, the mirror-reflecting system of forming images is employed in the eye of the scallop.

A completely opposing function to the reflector is also widely distributed in the animal world. A regularly structured surface works as an antireflector and enhances the optical transparency of the surface. Bernhard et al.<sup>[48]</sup> noticed that the surface of the compound eye of a night moth bore a hexagonal array of cone-shaped protuberances, corneal nipples, with a spacing and height of 170 and 200 nm, respectively. They considered the regular modulation of the surface as a refraction matching, and the reflectivity at the surface was found to decrease by two orders of magnitude compared with that of a non-nippled cornea. The developmental study revealed that the origin of the nipples came from the growth of regularly spaced microvilli. Further, the shape of the nipple was closely related to the magnitude of matching, which was confirmed by a corresponding microwave experiment. Yoshida<sup>[49–51]</sup> found that similar protuberances were present on the transparent wing of a hawk moth, *Cephonodes hylas* (Figure 20), and con-

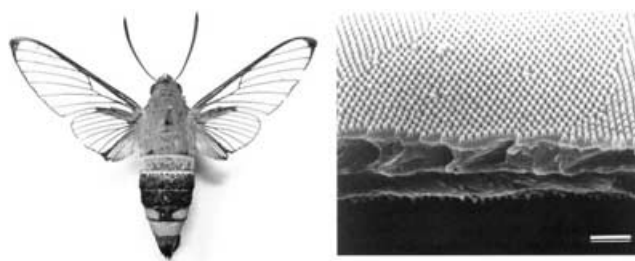


**Figure 20.** Electron microscopic image of a surface of the transparent wing of a hawk moth (wingspan = 55 mm), *Cephonodes hylas*.<sup>[49]</sup> Bar = 1  $\mu\text{m}$ .

firmed that the reflectivity was increased by rubbing the surface into an artificial smooth surface. The optical properties of such a surface structure having a regular and sub-wavelength scale can be treated approximately as a layer with an average refractive index of air and the medium, and thus the nipple array behaves as an antireflective coating for the surface.

## 5. Photonic-Crystal-Type Structural Color

At the beginning of the 20th century, Mason performed careful investigations on many kinds of bird feathers and discussed the similarities of their iridescent color to those of thin films.<sup>[10]</sup>

Later, electron microscopic investigations revealed a surprisingly minute structure in the feathers of peacock, hummingbirds, pheasant, and ducks. In these birds, melanin granules formed a submicron periodic structure with periodicity comparable to the wavelength of visible light, which was thought to be the origin of optical interference.<sup>[52–57]</sup>

These structures are now called photonic crystals. Studies on the interaction of electromagnetic waves with such periodic dielectric structures have been rapidly developing in this decade to investigate the existence of a photonic bandgap, where all electromagnetic waves are forbidden to propagate and even to exist within a crystal. Enormous efforts have been made, both theoretically and experimentally, to obtain a full photonic bandgap in two- (2D) and three-dimensional (3D) periodic structures. Thus, the major interest at present is how a complete photonic crystal is materialized from theoretical and experimental viewpoints. The development of this path of research is very similar to that of semiconductor science. On the other hand, in the natural world, a completely different concept emerged in the course of evolution, which causes the interaction between light and a periodic dielectric material. This interaction is mainly intended to stimulate the perception of creatures and hence irregularity of wide diversity is rather actively incorporated into a crystal. Thus, the goals of these two trends are completely different, although they have a common root.

Figure 21 shows an example of a “photonic crystal” in peacock.<sup>[56]</sup> A peacock feather consists of many barbs, each of which has a lot of branches called barbules. The barbules are

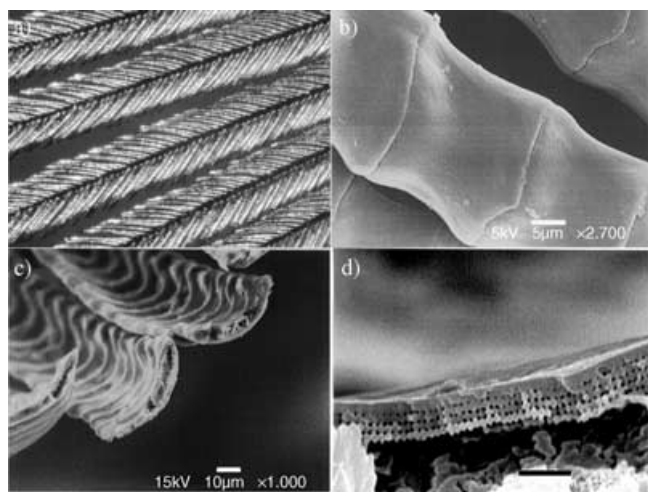


**Figure 21.** a) Optical and b–d) scanning electron microscopic images of barbules of a peacock feather.<sup>[56,57]</sup> The bars are b) 5, c) 10, and d) 1  $\mu\text{m}$ .

curved along its long axis and slightly twisted from its root. Each barbule has the shape of connected segments, typically 20–30  $\mu\text{m}$ , the surfaces of which are smoothly curved like a saddle. Microscopic investigation reveals that its transverse cross-section is crescent-shaped and the brilliant color comes from these segments in the barbule. Under high magnification, several layers consisting of periodically arrayed particles are

observed beneath the surface layer. This lattice structure consists of particles of 8–12 layers, whose diameters are reported to be 110–130 nm. The layer intervals are dependent on the color of the feather: 140–150, 150, and 165–190 nm for blue, green, and yellow feathers, respectively.<sup>[56,58]</sup> Below the lattice structure, the particles are rather randomly distributed. In contrast to the transverse direction, the particles have an elongated shape of length 0.7  $\mu\text{m}$ <sup>[58]</sup> with random arrangement in the longitudinal direction. The slender particles are melanin granules and cause the barbule to be dark brown when one sees through it. Thus, the photonic crystal in peacock forms a square lattice nearly in 2D. It is also noticed that the crescent-shaped barbule makes the lattice structure curved along the surface.

The optical properties of the peacock feather are well described by the above structural characteristics. The peak wavelength of the reflection spectrum under normal incidence is explained in terms of the lattice structure. The present authors<sup>[56]</sup> considered that an incident plane wave of light was scattered at each particle in 2D and the scattered light interfered in the far field under the assumption of a Rayleigh–Gans-like approximation. In this simulation, only four to eight layers are taken into account depending on the bandwidth, because the existence of melanin pigment has the function of reducing the effective number of layers. Zi et al.<sup>[58]</sup> calculated the photonic band structure of an infinite 2D photonic crystal with a square lattice and found a partial photonic bandgap along the  $\Gamma$ – $X$  direction for two polarization directions. Correspondingly, they calculated the reflectance spectra for finite numbers of layers adapted to the color of the feather and reproduced fairly well the reflection spectra from various barbules.

However, these simplified treatments do not reproduce the angular dependence of the reflection intensity correctly and, for a quantitative agreement, the crescent-shaped macroscopic structure superposed on the lattice structure should be taken into account. Introducing this effect by considering the distribution of the lattice orientations, the present authors<sup>[56]</sup> reproduced the angular dependence of the reflectance considerably well. Thus, both the regularity due to the photonic crystal and the irregularity corresponding to the macroscopic deformation coexist in addition to the pigment, which enhances the contrast of the coloring of the feather. The principles of structural color found in *Morpho* butterflies are again satisfied in peacock. Interestingly, the melanin pigment in peacock coexists with the regular structure, while in *Morpho* butterflies the pigment is distributed beneath the regular structure of the scale.

The photonic crystal-type structural colors have been widely reported in butterflies,<sup>[21–23,59–61]</sup> beetles,<sup>[62]</sup> and sea animals<sup>[63]</sup> (Figure 22). Ghiradella<sup>[21–23,60]</sup> reported various lattice structures in butterflies *Mitoura grynea*, *Teinopalpus imperialis*, *Parides sesostris*, and *Callophrys rubi*. In *Mitoura grynea*, granules formed a face-centered-cubic structure in the lower part of the scale, where a negative crystal is formed with the lattice point constituted by an air hole. Vukusic et al.<sup>[61]</sup> reported that in the iridescent scale of *Parides sesostris*, the neighboring and differently oriented domains with about 2  $\mu\text{m}$  size of identical 3D honeycombed lattice of voids were distributed in the lower part. This

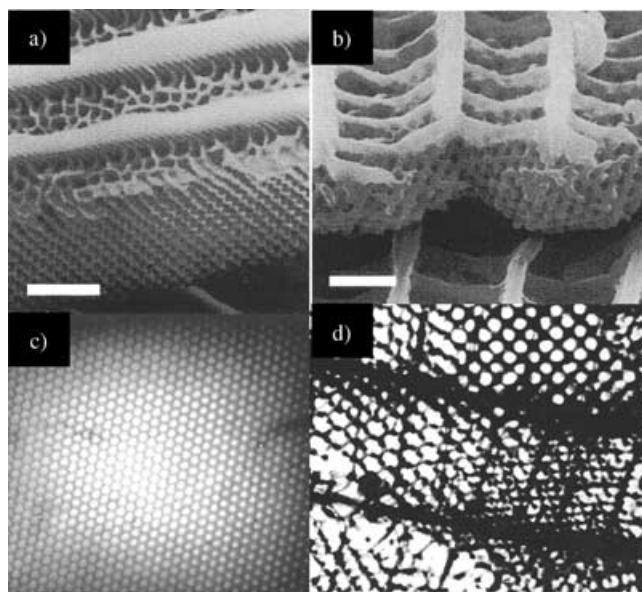


**Figure 22.** Photonic crystals found in various creatures; butterfly scales of a) *Teinopalpus imperialis*,<sup>[22]</sup> b) *Mitoura grynea*,<sup>[22]</sup> and d) *Callophrys rubi* (TEM  $\times 22\,000$ ),<sup>[20]</sup> and c) spine of a sea mouse with voids  $0.51\ \mu\text{m}$  apart, *Aphrodite* sp.<sup>[63]</sup> The bars are  $1\ \mu\text{m}$  for (a) and (b).

domain structure seems to be again one of the different expressions for the irregularity.

Parker et al.<sup>[62]</sup> reported the opal-type photonic crystal emitting the iridescent color from the scales of a weevil in Australia, *Pachyrhynchus argus*. They also reported that the spine of a sea mouse, marine annelid *Aphrodite* sp., was made from close-packed hollow cylinders  $0.51\ \mu\text{m}$  apart with the wall made of pure  $\alpha$ -chitin ( $n = 1.54$ ) and seawater inside the cylinder. They calculated the reflection spectrum and found a strong reflection at the blue and red regions,<sup>[63]</sup> which correspond to the partial photonic bandgap. Similar photonic crystal-type structural colors have been discovered one after another from various ranks of the animal world, and it has become one of the common expressions for structural color.

## 6. Organized Light Scattering in Structural Colors

Scattering of light is another source of structural colors, which is completely different from multilayer interference and/or the photonic crystal type, because it has its root in the irregularity of the structure. Light scattering has been thought to be a cause of blue coloring in a wide variety of random media. The origin of the blue sky was explained first by Lord Rayleigh as due to light scattering by atmospheric molecules. The color of the suspension involving small colloidal particles is called Tyndall blue. The blue color in these cases is based on the fact that the scattering cross-section is dependent on the fourth power of the frequency of light, and the scattered light at right angles is polarized to a large extent. Mie scattering occurs with increasing size of the particles, and the wavelength dependence differs considerably from that of Rayleigh scattering. Thus, a different coloration should appear. The most

famous example of Mie scattering is the coloration of the sunset on Mars, which is blue in contrast to red on Earth. The reason for this change of color is explained by the larger particles in the Mars atmosphere that scatter red rather than blue owing to Mie scattering.

Light scattering has often appeared in the literature as a typical example of structural colors. Mason<sup>[12]</sup> reported that the colors of some insects were due to Tyndall blue, and the body of a dragonfly, *Mesothemis simplicicollis*, and the wing of *Libellula pulchella* were exemplified. Huxley<sup>[64]</sup> implies that the color of the blue scale in an African butterfly, *Papilio zalmoxis*, is due partly to Tyndall scattering at a layer of air-filled alveoli and partly to thin-film interference at a basement lamella. Ghiradella<sup>[23]</sup> also referred to the butterfly scale of *P. oribazus*, similar to *P. zalmoxis*, as due to Tyndall blue. Parker et al.<sup>[65]</sup> explained the gradation from blue to white in terms of the relative sizes of particles which determine the shade of blue. He exemplified the wing of *L. pulchella* and the body of a dragonfly, *Orthetrum caledonicum*, as due to Tyndall scattering by minute colorless granules within epidermal cells located over a dark base. In spite of many descriptions of Tyndall blue in animals, there has been no report to measure quantitatively the wavelength dependence of the scattering cross-section and its polarization characteristics. Thus, the problem of whether pure Tyndall scattering determines their colors or not seems to be left behind.

On the other hand, it has been gradually clarified that light scattering is somehow organized and contributes effectively to the color. The spongy medullary keratin matrices found in the barb of bird feathers, for example parakeet and plum-throated cotinga, had been widely believed as due to Rayleigh scattering occurring at the interface of keratin ( $n = 1.54$ ) and air (see Figure 23, for example). However, this model failed to explain their reflection spectra because they have a peak from the

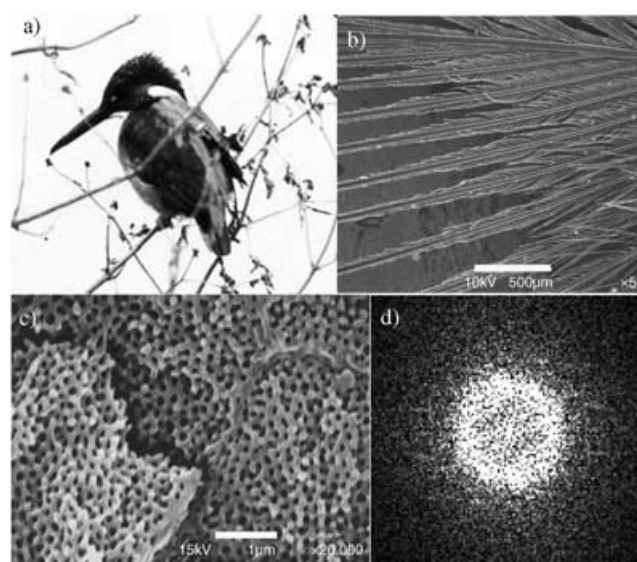


**Figure 23.** Spongy medullary matrix (c) found in b) the barb of a common kingfisher (body length =  $150\ \text{mm}$ ), *Alcedo atthis* [photographed by Matsu-miya] (a). The bars are b)  $500$  and c)  $1\ \mu\text{m}$ . d) 2D Fourier transform of the cross-section of a TEM image. The lengths of both sides of the image are  $18.5 \times 2\pi\ \mu\text{m}^{-1}$ . The radius of the circle corresponds to  $3.1 \times 2\pi\ \mu\text{m}^{-1}$ .

violet to blue region. Prum et al.<sup>[66]</sup> performed spatial Fourier transformation of the electron microscopic images and found a clear ring structure in the momentum space. If the spongy structure with a wide variety of sizes was distributed, a Gaussian-like distribution should be obtained, located at a center in the momentum space. The ring structure means the characteristic size of the matrix is rather uniform and is modeled by angularly distributed, broken multilayers, whose layer thickness is coincident with the widths of the air hole and keratin bridge. They also examined the similar structures in avian skins of various species,<sup>[67]</sup> which appeared as quasi-ordered arrays of parallel collagen fibers, and found a similar spatial order. These findings are very important because the seemingly random structure of the spongy matrix actually has a uniform characteristic size, which changes the incoherent light scattering into coherent scattering, with enforcing reflection to a large extent. Thus, structural colors due to irregular structure are enforced by incorporating a regular structure inside.

Similar schemes were also found in the layer structures located at the lower part of the scale of butterflies, family Licaenidae (Figure 24). Tilley and Eliot<sup>[68]</sup> investigated the scales of

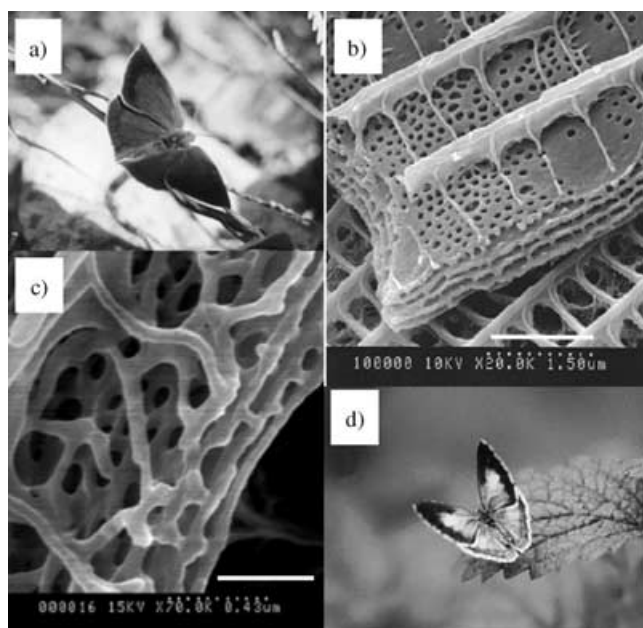


**Figure 24.** Scanning electron microscopic images of iridescent scales of licaenid butterflies. a,b) *Narathura japonica japonica* (wingspan ~50 mm) and c,d) *Celastrina argiolus ladonides* (wingspan ~35 mm) [photographed by Matsumiya]. The bars are b) 1.5 and c) 0.43  $\mu\text{m}$ .

various licaenid butterflies using SEM and found a wide variety of layers in the scales. These are layers of a network structure as in *Celastrina argiolus*, of wrinkled planes as in *Eumaeus minijas*, of planes with holes as in *Ancema blanka* and so on. In these scales, the diffusive light is produced through light scattering by irregular structures, and through the diffraction of light by wrinkles or holes, which is then enforced selectively in angle and wavelength owing to attached layer structures through interference.

## 7. Summary and Outlook

### 7.1. Summary of Structural Colors in Nature

We have overviewed the mechanisms and distributions of the structural colors from a viewpoint of regularity and irregularity within their structures. As a result, we can classify the structural colors into two categories according to their structural origins. First, they originate from the regular structure, which has a dimension slightly less than the wavelength of light, and the irregular structure, which is much larger than the former and contributes to emit the diffusive light. The multilayer interference and photonic crystal types (e.g., *Morpho* butterfly) belong to this category. Second, the structural color originates from the irregular structure, which generally has a dimension smaller than or comparable to the wavelength of light and contributes to emit diffusive light. On the other hand, the regular structure, the periodicity of which is slightly smaller than the wavelength, persists over a much larger region to enforce the reflection of light selectively in angle and wavelength. The organized light scattering (e.g., lycaenid butterfly) described above may be classified in this category.

To make the structural color effective for perception by the eye, it is necessary to have a certain kind of enforcing process such as multilayer interference or a photonic crystal, where multiple reflection occurs. In this sense, simple optical processes such as thin-film interference and/or light scattering are rather difficult to stand by themselves. On the contrary, diffraction grating-type structural color is rare in nature, although it has an enforcing process due to the periodic structure of the grating. This is probably because it does not insist on a specific color but rather shows the variation of colors, which may not adapt to the purposes of animals, although in ancient days 515 million years ago, creatures bearing iridescent color due to a diffraction grating effect were reported to be present.<sup>[65]</sup>

Naturally, the above classification is not strict and is sometimes complicated because it is difficult to determine which has a priority, when the characteristic sizes of these structures become comparable. However, if they have very different sizes, their roles should become clear. We illustrate the characteristic sizes for several typical animals bearing structural color in Figure 25. The most important is a periodicity of the structure causing interference, which becomes roughly on the order of half a wavelength. Second is a persistent length or area in which such periodicity is sustained. When the length is too small, the wave nature of light such as diffraction becomes important, whereas the geometrical optics is dominant when the length becomes much larger. The third and higher order of the features may characterize the distribution of such structures, and so on. Thus, the hierarchy of the structure is a common feature in these animals. Although the physical meaning of such structural hierarchy is not clear, if such hierarchical structures display a unique effect on vision in each hierarchy, the structural colors could not be mentioned without it.

However, even in the case of irregularity-based structural colors, similar hierarchy seems to be present. The persistence length of the regularity is large for the lycaenid butterflies,

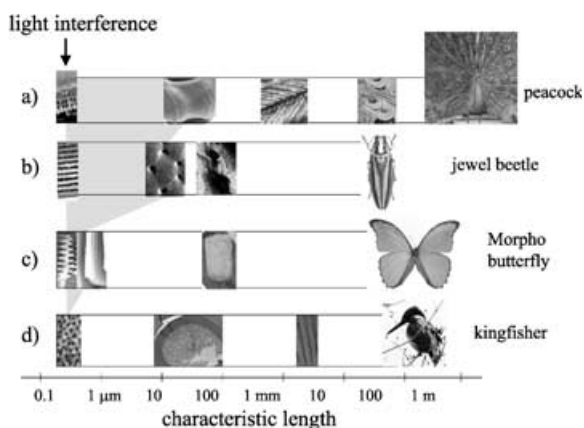


**Figure 25.** Hierarchy of the structure contributing to structural colors. The most fundamental scale is that giving the interference of light around  $0.2 \mu\text{m}$ . The regular structures contributing to the light interference are retained within a range indicated as a gray zone. If this range is narrow, the diffraction of light plays an important role, whereas if broad, the geometrical optics dominates. In either case, this range helps to produce diffusive light. The hierarchy in a larger scale indicates the irregularity at various levels and possibly adds the macroscopic texture to the structural color.

while in the spongy medullar structures found in bird feathers, it is rather difficult to discriminate between the size of the irregularity and the persistence length of the regularity. Although the classification due to the regularity and irregularity considering the hierarchy of the structure is just beginning, it will offer important information on the developmental and ethological studies.

## 7.2. Industrial Applications and Outlook

Structural colors have been closely connected with human life since the dawn of civilization. They have often been used for ornaments and decoration of accessories and furniture. Opal and pearl are one of the most well-known natural jewels utilizing structural color. In Japan, the wings of jewel beetles and the feathers of birds were used for decoration more than a thousand years ago. A Buddhist miniature temple decorated by the wings of jewel beetles all over the pillars, built in the 7th century, is the most famous in Japan. Use of the lamina of mother-of-pearl of ear shell or turban shell to decorate lacquerware was brought from China in the 8th century. In Ukiyoe, which flourished in the 17–18th centuries, mica powder was employed to express the gloss of the background for the portrait.

The structural color used for decoration in olden days was employed as it was or only after minor processing. However, industrial requirements to enhance its brilliancy have been rapidly increasing in this decade. Most of the materials showing structural color are processed to a powder and are used after mixing with pigment. The famous one is “pearl pigment”, in which mica flakes are coated by  $\text{TiO}_2$  film to increase the reflectivity at the interface. Because of the wide band and low reflectance of each flake, pileup of the flakes is necessary to increase the reflectivity, which causes its profound, pearlescent luster. To increase the reflectivity and wavelength selectivity,

the thickness of the  $\text{TiO}_2$  layer is adjusted to match the thin-film interference condition, which is called “interference pearl pigment”. To enhance the effect much more, a new pigment called “optically variable pigment” has appeared, which utilizes a silica flake covered with a high-reflection metal coating. This type of pigment shows highly metallic reflectivity and strong color changes with changing viewing angle.

In the textile world, a more sophisticated fiber was invented by Iohara et al.<sup>[69]</sup> through mimicking the scale structure of the *Morpho* butterfly. This fiber is made of polyester and has a flattened shape of thickness  $15\text{--}17 \mu\text{m}$ , in which 61 layers of nylon 6 and polyester with a thickness of  $70\text{--}90 \text{ nm}$  are incorporated (Figure 26). Because of the multilayered structure,

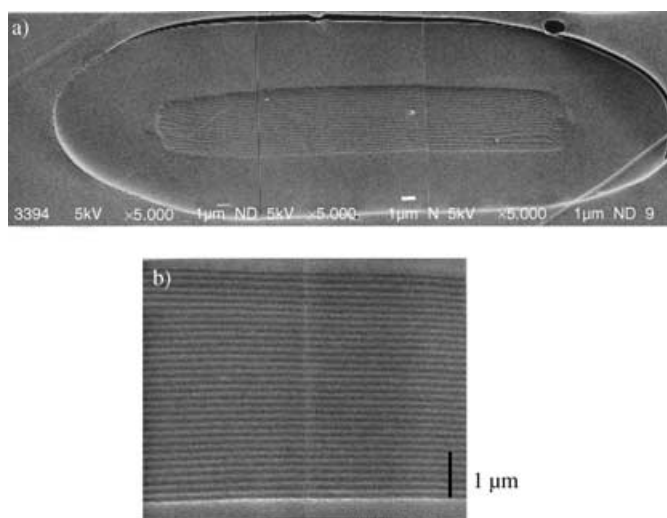


**Figure 26.** a) Scanning microscopic image of the cross-section of a flattened polyester fiber mimicking *Morpho* butterfly. b) The fiber includes 61 alternate layers of nylon 6 and polyester with a thickness of  $70\text{--}90 \text{ nm}$ .<sup>[69]</sup> Bar =  $1 \mu\text{m}$  [Courtesy of Teijin Fibers Limited].

wavelength-selective reflection and a change with viewing angle are obtained. Moreover, the flat shape of the fiber makes it possible to align the direction of the multilayer, which increases the effective reflectivity. These properties were demonstrated by weaving a wedding dress using this fiber. However, since the polymer materials constituting the layers have similar refractive indices, the range of high reflectance is limited within a small wavelength region, which differs considerably from the *Morpho* butterfly.

Saito and our group have fabricated a *Morpho* substrate to utilize the principle of its structural color.<sup>[70,71]</sup> Using dry etching by an electron-beam technique, we fabricated a substrate of  $6 \times 6 \text{ mm}^2$  dimension, in which tips of a unit of  $0.3 \times 2 \mu\text{m}$  are arranged in a plane. The lengths of the short and long sides correspond to the width of the ridge and the average length between the adjacent upper ends of the lamellae in a ridge, respectively. To express the random height of the ridge, the height of the unit has a two-valued random variable. The difference of the height is adjusted at  $0.11 \mu\text{m}$  to make the destructive interference for the normally reflected light of

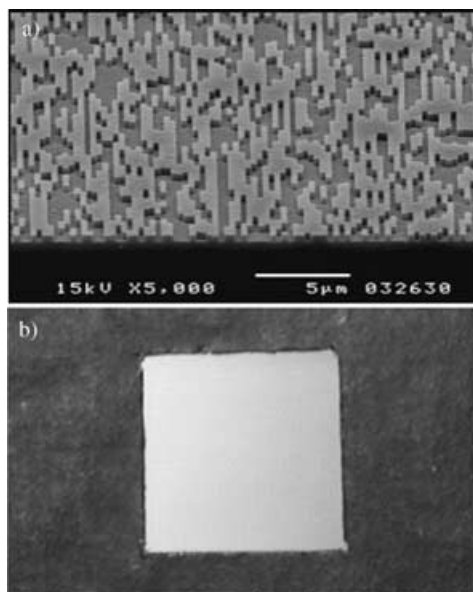


**Figure 27.** a) Scanning electron microscopic image of a glass substrate, whose surface is processed with randomly distributed tips of size  $0.3 \times 2 \mu\text{m}^2$  and a two-valued random height of 0 or  $0.11 \mu\text{m}$ . b) Multilayer coating consisting of  $\text{SiO}_2$  and  $\text{TiO}_2$  on the substrate ( $6 \times 6 \text{ mm}^2$ ) reveals a brilliancy similar to that of the *Morpho* wing.<sup>[70]</sup> Bar =  $5 \mu\text{m}$ .

$0.44 \mu\text{m}$ . The SEM image for the fabricated substrate is shown in Figure 27a. Evaporation of 14 alternate layers of  $\text{SiO}_2$  ( $n = 1.47$ ) and  $\text{TiO}_2$  ( $n = 2.4$ ) resulted in high reflectivity with a broad bandwidth. As shown in Figure 27b, the substrate thus fabricated resembles the *Morpho* wing with respect to the reflectivity, color, bandwidth, angular dependence, and anisotropy. It is easily understood that this approach does not mimic the structure of the *Morpho* scale itself, but only its principle due to the cooperation of regularity and irregularity. In other words, the success of the reproduction based on this principle verifies the correctness of the understanding of the structural color in the *Morpho* butterfly.

A completely different approach to mimicking the scale of the *Morpho* butterfly is being advanced by Matsui et al.,<sup>[72]</sup> who utilize a focused ion-beam-chemical vapor deposition (FIB-CVD) technique to reproduce the complete structure of

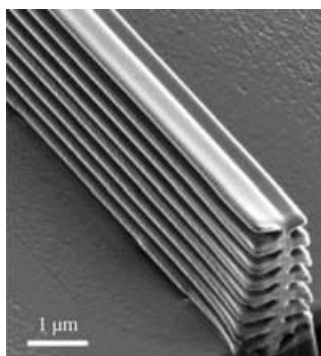


**Figure 28.** Ridge structure mimicking the *Morpho* scale, fabricated by a focused-ion-beam-chemical vapor deposition (FIB-CVD) technique.<sup>[72]</sup> Bar =  $1 \mu\text{m}$ .

the ridge. They have made the distance of lamellae so adjusted to agree with that of the *Morpho* butterfly and even to reproduce the alternate structure of the lamella as described above (Figure 28). The replica illuminated by white light is found to actually glitter blue to violet under microscopic observation. Thus, recent rapidly developing nanotechnology proves that even the most elaborate structure in nature comes true. Therefore, the future of the study of structural colors is extremely promising, because the optical and physical investigation of their mechanisms will be immediately confirmed by fabricating reproductions directly and from first principles.

**Keywords:** iridescence · optical properties · structural color · thin films

- [1] R. Hooke, *Micrographia*, reprinted by Dover Publications, Inc., New York, **2003**.
- [2] I. Newton, *Opticks*, reprinted by Dover Publications, Inc., New York, **1952**, p. 252.
- [3] B. Walter, *Die Oberflächen-oder Schillerfarben*, Braunschweig, **1895**.
- [4] A. A. Michelson, *Philos. Mag.* **1911**, *21*, 554–567.
- [5] Lord Rayleigh, *Roy. Soc. Proc.* **1917**, *A93*, 565–577.
- [6] Lord Rayleigh, *Philos. Mag.* **1919**, *37*, 98–121.
- [7] Lord Rayleigh, *Roy. Soc. Proc.* **1923**, *A103*, 233–239.
- [8] H. Onslow, *Philos. Trans. R. Soc. Lond.* **1921**, *B211*, 1–74.
- [9] E. Merritt, *J. Opt. Soc. Am. Rev. Sci. Instrum.* **1925**, *11*, 93–98.
- [10] a) C. W. Mason, *J. Phys. Colloid Chem.* **1923**, *27*, 201–251; b) C. W. Mason, *J. Phys. Chem.* **1923**, *27*, 401–447.
- [11] C. W. Mason, *J. Phys. Chem.* **1926**, *30*, 383–395.
- [12] C. W. Mason, *J. Phys. Chem.* **1927**, *31*, 321–354.
- [13] C. W. Mason, *J. Phys. Chem.* **1927**, *31*, 1856–1872.
- [14] M. F. Land, *Prog. Biophys. Mol. Biol.* **1972**, *24*, 75–106.
- [15] A. F. Huxley, *J. Exp. Biol.* **1968**, *48*, 227–245.
- [16] M. Born, E. Wolff, *Principles of Optics*, Pergamon, New York, **1959**.
- [17] K. Sakoda, *Optical Properties of Photonic Crystals*, Springer, Berlin, **2001**.
- [18] C. M. Penz, P. J. DeVries, *American Museum Novitates*, No. 3374, American Museum of Natural History, New York, **2002**.
- [19] T. F. Anderson, A. G. Richards, Jr., *J. Appl. Phys.* **1942**, *13*, 748–758.
- [20] H. Ghiradella, W. Radigan, *J. Morphol.* **1976**, *150*, 279–298.
- [21] H. Ghiradella, *Ann. Entomol. Soc. Am.* **1984**, *77*, 637–645.
- [22] H. Ghiradella, *Appl. Opt.* **1991**, *30*, 3492–3500.
- [23] H. Ghiradella, *Microsc. Res. Tech.* **1994**, *27*, 429–438.
- [24] H. Ghiradella in *Microscopic Anatomy of Invertebrates*, Vol. 11A (Eds.: F. W. Harrison, M. Locke), Wiley-Liss, New York, **1998**, pp. 257–287.
- [25] H. Ghiradella, *J. Morphol.* **1974**, *142*, 395–410.
- [26] H. Ghiradella, *J. Morphol.* **1989**, *202*, 69–88.
- [27] H. Tabata, K. Kumazawa, M. Funakawa, J. Takimoto, M. Akimoto, *Opt. Rev.* **1996**, *3*, 139–145.
- [28] P. Vukusic, J. R. Sambles, C. R. Lawrence, R. J. Wootton, *Proc. R. Soc. Lond. B* **1999**, *B266*, 1403–1411.
- [29] S. Kinoshita, S. Yoshioka and K. Kawagoe, *Proc. R. Soc. Lond. B* **2002**, *B269*, 1417–1421.
- [30] S. Kinoshita, S. Yoshioka, Y. Fujii, N. Okamoto, *Forma* **2002**, *17*, 103–121.
- [31] S. Yoshioka, S. Kinoshita, *Proc. R. Soc. Lond. B* **2004**, *B271*, 581–587.
- [32] A. C. Neville, *J. Insect Physiol.* **1977**, *23*, 1267–1274.
- [33] a) M. Kurachi, Y. Takaku, Y. Komiya, T. Hariyama, *Naturwissenschaften* **2002**, *89*, 295–298; b) T. Hariyama, Y. Takaku, M. Hironaka, H. Horiguchi, Y. Komiya, M. Kurachi, *Forma* **2002**, *17*, 123–132.
- [34] S. Kinoshita, *Cell Tech.* **2003**, *22*, 1113–1119 (in Japanese).
- [35] T. Hariyama, private communication.
- [36] A. C. Neville, S. Caveney, *Biol. Rev.* **1969**, *44*, 531–562.
- [37] S. Kinoshita, S. Yoshioka, Y. Fujii, *J. Jpn. Soc. Color Mater.* **2002**, *75*, 493–499.
- [38] D. W. Lee, *Am. Sci.* **1997**, *85*, 56–63.
- [39] W. Lippert, K. Gentil, *Z. Morphol. Oekol. Tiere* **1959**, *48*, 115–122.

- [40] a) P. Vukusic, J. R. Sambles, C. R. Lawrence, *Nature* **2000**, *404*, 457; b) P. Vukusic, R. Sambles, C. Lawrence, G. Wakely, *Appl. Opt.* **2001**, *40*, 1116–1125.
- [41] H. Tada, S. E. Mann, I. N. Miaoulis, P. Y. Wong, *Appl. Opt.* **1998**, *37*, 1579–1584.
- [42] a) H. Nagaishi, N. Oshima, R. Fujii, *Comp. Biochem. Physiol.* **1990**, *95A*, 337–341; b) H. Nagaishi, N. Oshima, *Zool. Sci.* **1992**, *9*, 65–75.
- [43] E. B. Poulton, *Trans. Ent. Soc. Lond.* **1888**, 515.
- [44] a) R. A. Steinbrecht, W. Mohren, H. K. Pulker, D. Schneider, *Proc. R. Soc. Lond. B* **1985**, *B226*, 367–390; b) R. A. Steinbrecht, *Tissue Cell* **1985**, *17*, 745–762.
- [45] a) E. Denton, *Sci. Am.* **1971**, *224*, 64–72; b) E. Denton, *Proc. R. Soc. Lond. B* **1971**, *B178*, 43–61.
- [46] a) M. F. Land, *Sci. Am.* **1978**, *239*, 88–99; b) M. F. Land, *J. Opt. A Pure Appl. Opt.* **2000**, *2*, R44–R50.
- [47] A. R. Parker, *Am. Sci.* **1999**, *87*, 248–253.
- [48] a) C. G. Bernhard, W. H. Miller, A. R. Moller, *Acta Physiol. Scand.* **1965**, *63* (Suppl. 243), 1–79; b) C. G. Bernhard, W. H. Miller, A. R. Moller, *Quart. Rev. Biophys.* **1968**, *1*, 89–105; c) W. H. Miller, A. R. Moller, C. G. Bernhard in *The Functional Organization of the Compound Dye* (Ed.: C. G. Bernhard), Pergamon Press, Oxford, **1966**.
- [49] A. Yoshida, M. Motoyama, A. Kosaku, K. Miyamoto, *Zool. Sci.* **1996**, *13*, 525–526.
- [50] A. Yoshida, *Forma* **2002**, *17*, 75–89.
- [51] A. Yoshida, M. Motoyama, A. Kosaku, K. Miyamoto, *Zool. Sci.* **1997**, *14*, 737–741.
- [52] C. H. Greenwalt, W. Brandt, D. D. Friel, *J. Opt. Soc. Am.* **1960**, *50*, 1005–1013.
- [53] H. Durrer, *Verh. Naturf. Ges. Basel* **1962**, *73*, 204–224.
- [54] W. J. Schmidt, H. Ruska, *Z. Zellforsch. Mikrosk. Anat.* **1962**, *57*, 1–36.
- [55] E. Rutschke, *Z. Zellforsch. Mikrosk. Anat.* **1966**, *73*, 432–443.
- [56] S. Yoshioka, S. Kinoshita, *Forma* **2002**, *17*, 169–181.
- [57] S. Yoshioka, *O plus E* **2001**, *23*, frontispiece (in Japanese).
- [58] J. Zi, X. Yu, Y. Li, X. Hu, C. Xu, X. Wang, X. Liu, R. Fu, *Proc. Natl. Acad. Sci. USA* **2003**, *100*, 12576–12578.
- [59] R. B. Morris, *J. Ent. A* **1975**, *49*, 149–154.
- [60] H. Ghiradella, *Ann. Entomol. Soc. Am.* **1985**, *78*, 252–264.
- [61] P. Vukusic, J. R. Sambles, *Nature* **2003**, *424*, 852–855.
- [62] A. R. Parker, V. L. Welch, D. Driver, N. Martini, *Nature* **2003**, *426*, 786–787.
- [63] a) A. R. Parker, R. C. McPhedran, D. R. McKenzie, L. C. Botten, N.-A. P. Nicorovici, *Nature* **2001**, *409*, 36–37; b) R. C. McPhedran, N. A. Nicorovici, D. R. McKenzie, L. C. Botten, A. R. Parker, G. W. Rouse, *Aust. J. Chem.* **2001**, *54*, 241–244.
- [64] a) J. Huxley, *J. Entomol.* **1975**, *50*, 9–22; b) J. Huxley, *Proc. R. Soc. Lond. B* **1976**, *B193*, 441–453.
- [65] A. R. Parker, *J. Opt. A* **2000**, *2*, R15–R28.
- [66] a) R. O. Prum, R. H. Torres, S. Williamson, J. Dyck, *Nature* **1998**, *396*, 28–29; b) R. O. Prum, R. H. Torres, S. Williamson, J. Dyck, *Proc. R. Soc. Lond.* **1999**, *B266*, 13–22.
- [67] R. O. Prum, R. Torres, *J. Exp. Biol.* **2003**, *206*, 2409–2429.
- [68] R. J. D. Tilley, J. N. Eliot, *Trans. Lepid. Soc. Jpn.* **2002**, *53*, 153–180.
- [69] K. Iohara, M. Yoshimura, H. Tabata, S. Shimizu, *Chem. Fibers Int.* **2000**, *50*, 38–39.
- [70] S. Yoshioka, S. Kinoshita, A. Saito, *Oyo Butsuri* **2004**, *73*, 939–942.
- [71] A. Saito, S. Yoshioka, S. Kinoshita, *Proc. SPIE* **2004**, *5526*, 188–194.
- [72] K. Watanabe, T. Hoshino, K. Kanda, Y. Haruyama, S. Matsui, *Jpn. J. Appl. Phys.* **2005**, *44*, L48–L50.

---

Received: January 5, 2005

Published online on July 14, 2005